Magnetic Hysteresis Properties of Magnetite: Trends with Particle Size and Shape

Greig A. Paterson[1], Roberto Moreno[2,3], Adrian R. Muxworthy[4], Lesleis Nagy[1], Wyn Williams[2], and Lisa Tauxe[5]

[1]Department of Earth, Ocean and Ecological Sciences, University of Liverpool, Liverpool, UK.
[2]School of GeoSciences, University of Edinburgh, Edinburgh, UK.
[3]Instituto de Física Enrique Gaviola, Ciudad Universitaria, Córdoba, Argentina
[4]Department of Earth Science and Engineering, Imperial College London, London, UK.
[5]Scripps Institution of Oceanography, La Jolla, CA. USA

Key Points:

- Magnetic hysteresis is micromagnetically modeled for oblate, prolate and equant magnetite particles (50-195 nm).
- The reduced magnetization (M_{rs}/M_s) is a very effective parameter for differentiating between magnetically single-domain and non-single-domain behavior.
- Transient magnetic hysteresis is a powerful tool for identifying stable remanent magnetizations, but is currently infrequently reported.

Corresponding author: Greig A. Paterson, greig.paterson@liverpool.ac.uk

Abstract

Magnetic hysteresis measurements are routinely made in the Earth and planetary sciences to identify geologically meaningful magnetic recorders, and to study variations in present and past environments. Interpreting magnetic hysteresis data in terms of domain state (particle size) and paleomagnetic stability are major motivations behind undertaking these measurements, but the interpretations remain fraught with challenges and ambiguities. To shed new light on these ambiguities, we have undertaken a systematic micromagnetic study to quantify the magnetic hysteresis behavior of room-temperature magnetite as a function of particle size (50-195 nm; equivalent spherical volume diameter) and shape (oblate, prolate and equant); our models span uniformly magnetized single domain (SD) to non-uniformly magnetized single vortex (SV) states. Within our models the reduced magnetization marks a clear boundary between SD ($\geq$0.5) and SV ($<$0.5) magnetite. We further identify particle sizes and shapes with unexpectedly low coercivity and coercivity of remanence. These low coercivity regions correspond to magnetite particles that typically have multiple possible magnetic domain states, which has been previously linked to a zone of unstable magnetic recorders. Of all hysteresis parameters investigated, transient hysteresis is most sensitive to particles that exhibit such domain state multiplicity, leading us to suggest that transient behavior be more routinely measured during rock magnetic investigations.

Plain Language Summary

Characterizing the magnetic properties and behavior of natural materials is key in Earth and planetary sciences to identifying reliable magnetic recorders and variations in the environment. One standard method for achieving this is through room-temperature magnetic hysteresis measurement. However, the interpretation of magnetic hysteresis data remains one of the most challenging aspects of rock magnetism. To improve our understanding of magnetic hysteresis data, we have systematically investigated how the hysteresis properties of distributions of randomly oriented magnetite change as a function of particle size and shape and how this can help us quantify the contents of natural materials and identify rocks that may given unreliable magnetic signals. We model prolate, oblate and equant magnetite particles in the size range 50-195 nm. We show that magnetic hysteresis defines a clear boundary between simple uniform magnetic structures and more complex non-uniform magnetic structures. We also identify sizes and morphologies of magnetic particles that are likely to have unstable remanent magnetizations. These unstable particles are associated with distinctive hysteresis behavior, suggesting hysteresis data can be used to easily identify rock samples dominated by such behavior.

1 Introduction

Due to the relative ease and rapidity of measurement, magnetic hysteresis is a widely used technique in paleo-, rock, and environmental magnetic analysis and underpins assertions around magnetic particle size and paleomagnetic stability (*e.g.,* Dunlop, 2002; Day et al., 1977; Paterson et al., 2017). Despite the ease of measurement, processing and analyzing hysteresis data can be complicated (*e.g.,* Jackson & Solheid, 2010; Paterson et al., 2018), and the ubiquity of hysteresis data can lead to simplified or mis-interpretations of what these data mean when dealing with magnetically complex materials (*e.g.,* Roberts et al., 2018). Recent literature has highlighted the challenges of using hysteresis data for domain state identification (*e.g.,* Roberts et al., 2018); however, other work has suggested that hysteresis data have utility in quantifying the relative stability of paleomagnetic recorders (*e.g.,* Paterson et al., 2017). Some hysteresis experiments, such as determining First Order Reversal Curves, FORCs (Roberts et al., 1995a), are quite time consuming while others, such as measuring only the outer loops or just the transient hysteresis (Fabian, 2003; Yu & Tauxe, 2005), are fast. Hence, there is a trade-off between in-depth and time consuming measurements and analyses to decompose bulk specimen properties and the more rapid quantification of bulk hysteresis behavior and implications for other magnetic properties that are measured on bulk specimens (*e.g.,* paleomagnetic directions or paleointensities). Nevertheless, in both types of experiments, a comprehensive understanding of particle level hysteresis behavior is required to be able to fully interpret hysteresis data.

Although extensive experimental observations of magnetic hysteresis in sized particles of (nominally) magnetite have been made (*e.g.,* Day et al., 1977; Argyle & Dunlop, 1990; Krása et al., 2009), there are challenges in constraining particle size distributions, maintaining a single mineralogy, as well as preventing magnetostatic interactions between particles. There also remains the unquantified, and highly variable, particle geometry of these synthetic samples, which can play a notable role in their hysteresis properties (Williams et al., 2006).

Williams et al. (2006) and Yu & Tauxe (2008) explored hysteresis in magnetite as a function of particle geometry, where configurational anisotropy has a large, or dominant, control on the net anisotropy. They both illustrated that angular geometries tend to have higher coercivities due to the "pinning" effect of sharp surface angles. Yu & Tauxe (2008) further explored the influence of particle elongation (*i.e.,* shape anisotropy) for prolate cuboid and octahedral particles that exhibited single vortex (SV) states when equidimensional. As aspect ratio increases, B_c and M_{rs}/M_s initially increase due to a close balance between magnetocrystalline and shape anisotropy. As aspect ratio increases further, above $\sim$1.2, shape anisotropy dominates and both B_c and M_{rs}/M_s increase.

These works are based are low resolution finite difference models, whose domain structures are indicative, but the coercivities are far more sensitive to model resolution and edge effects. The characteristic hysteresis signals of isolated particles of varying size, shape, and composition are therefore not comprehensively understood, neither experimentally, nor micromagnetically.

In this work, we take a micromagnetic approach to systematically map out magnetic hysteresis behavior as a function of size and shape of isolated particles of magnetite. Unlike Williams et al. (2006) and Yu & Tauxe (2008), we explore the effects of particle shape at all particle sizes (up to 195 nm), and include oblate particle shapes, which were not part of the previous works. We evaluate the relative changes of common hysteresis parameters and what these mean in relation to magnetic domain states and magnetic stability of the modeled particles. Before introducing our micromagnetic models, we start with an overview of magnetic hysteresis and the main parameters derived from these data.

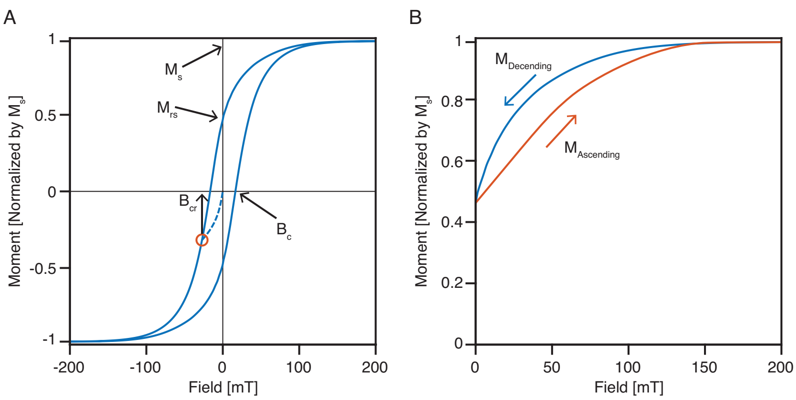

Figure 1. (A) Illustration of a hysteresis loop and associated parameters. The solid blue curve shows a hysteresis loop and the dashed blue curve s the back-field demagnetization curve used to determine the coercivity of remanence (B_{cr}). See text for description of the remaining parameters. (B) Illustration of a transient hysteresis loop whereby the descending loop from saturation is terminated at zero field and the field is then increased back to saturation. The transient hysteresis of Fabian (2003) is twice the area between the two curves, which accounts for the transient behavior in the negative field half of the hysteresis loop.

2 Hysteresis Measurement and Derived Properties

A hysteresis loop is initiated by saturating a specimen's magnetization in a large field, typically, $>$ 300 mT for magnetically soft materials or $\gg$ 1-10 T for magnetically hard materials (Figure 1A). From the saturated magnetization (M_s) state, the field is gradually reduced to the equivalent negative saturating field and swept back to positive saturation to complete the loop. The magnetization at the zero-field point is known as the saturation remanent magnetization (M_{rs}).

During the field sweep, a single domain (SD) magnetic particle will experience a critical switching of its magnetization to negative saturation as the field sweeps through a critical field, know as the coercivity (B_c). For larger particles, which do not have a uniform magnetic state, such as SV states (Schabes & Bertram, 1988; Williams & Dunlop, 1989), can experience changing domain states with changing field and switching of the magnetization may occur as a number of discrete steps caused by nucleation and denucleation of more complicated magnetization structures like the single vortex (*e.g.,* Williams & Dunlop, 1995; Lascu et al., 2018).

A number of other properties can be derived from a hysteresis loop by comparing the upper and lower branches (*e.g.,* Rivas et al., 1981; Fabian, 2003). The average and the difference of the upper and lower branches, are the induced and remanent hysteretic branches, respectively (Rivas et al., 1981; von Dobeneck, 1996; Paterson et al., 2018). The fields at which these curves fall to half of their peaks values represent the median destructive field in the induced and remanent branches, B_{ih} and B_{rh}, respectively (von Dobeneck, 1996; Fabian & von Dobeneck, 1997).

Fabian (2003) quantified the shape of a hysteresis loop, σ_{hys}, which is the log of the ratio of area of the loop to the area of the equivalent square hysteron for the observed M_s and B_c. A σ_{hys} value of zero indicates that the two loops have an equivalent area, hence, similar shape. Positive values are indicative of "pot-bellied" loops and negative values indicative of "wasp-waisted" loop (Tauxe et al., 1996). Deviations from a σ_{hys} of zero are often interpreted as being indicative of particle populations with distinct coercivities arising from the mixing of different particle sizes or different mineralogies (*e.g.,* Roberts et al., 1995a; Tauxe et al., 1996).

In a typical suite of rock magnetic measurements, additional data are often acquired to characterize the properties of a specimen. One such measurement is the back-field demagnetization curve; also known as a DC demagnetization curve. In a back field measurement, a specimen is initially in the positive remanent saturation state (M_{rs}). A small negative field is applied then removed and the magnetization is allowed to relax to a remanent state, which should be partially demagnetized with respect to the initial positive remanent saturation state. The negative, or back-field, is progressively increased until the specimen reaches the negative remanent saturation state. The field at which the remanent magnetization falls to zero is called the coercivity of remanence (B_{cr}). For an isolated SD particle switching of remanence will occur in a single critical switching at B_{cr}. For non-SD particle the switching of remanence states can occur in multiple discrete switches linked to changing domain structure.

An important point to note, is that while for SD particles, B_c and B_{cr} generally represent critical switching fields, for SV states, B_{cr} is a critical switching field, but B_c may not be. That is, application of B_{cr} field represents an irreversible switch in the magnetization, while the magnetization at B_c may, in some case, be reversible.

Transient hysteresis, T_{hys} (Figure 1b, which takes a specimen from positive saturation to the saturation remanent state (part of the major hysteresis branch) and then back to the positive saturation state (a minor hysteresis curve), is the area mapped out by difference in these two hysteresis branches (Fabian, 2003; Yu & Tauxe, 2005). T_{hys} is quantified as the ratio of the transient area to the area of the whole hysteresis loop (Fabian, 2003). In a uniformly magnetized SD particle, the field sweep has not passed the critical switching field represented by B_c, so the magnetization from the remanence state back to saturation is completely reversible. Hence, SD particles exhibit zero T_{hys}. In non-SD particles, the progressive switching steps during the field sweep caused by domain states changes in the return from remanence to saturation can be irreversible and result in substantial T_{hys}. In SV domain states, transient hysteresis is caused by vortex nucleation and annihilation occurring at different fields as the field is swept down from saturation and then back up, respectively (Figure 1c) (Yu & Tauxe, 2005; Zhao et al., 2017). T_{hys} is, therefore, indicative of complex and field history dependent domain state. Although straightforward and relatively quick to measure, transient hysteresis is typically not measured in most suites of rock magnetic measurements.

3 Methods

In this study we micromagnetically model hysteresis loops, transient hysteresis loops, and back-field demagnetization curves as a function of particle size and aspect ratio (AR = length/width) for magnetite at room temperature (20°C). The models were generated using the micromagnetic simulation software MERRILL v1.8.6p (Ó Conbhuí et al., 2018; Williams et al., n.d.), with truncated-octahedral geometries created using Coreform Trelis 17.1 (Coreform LLC, 2017), meshed at a resolution of 8 nm, which is below the exchange length of magnetite (Rave et al., 1998). In total, we model 16 particle sizes between 45 and 195 nm (expressed as the equivalent spherical volume diameter, ESVD) and aspect ratios between 0.17 (oblate) and 2.75 (prolate) (Figure 2). Prolate geometries were elongated along the $\langle 100 \rangle$ axis and oblate geometries were shortened along $\langle 100 \rangle$.

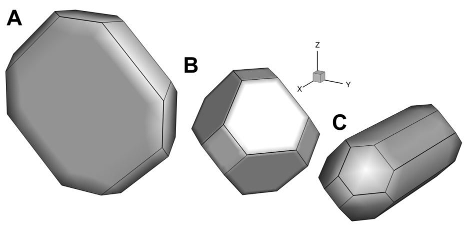

Figure 2. Examples of the range of geometries modeled in this study. Particles with an ESVD of 45 nm representing (A) oblate (AR = 0.17), (B) equant (AR = 1.00), and (C) prolate (AR = 2.75) geometries.

The simulated experiments were undertaken in fields between ±200 mT at 1 mT resolution, with hysteresis loops initiated at positive saturation. For hysteresis loops, only the upper branches were simulated, but through rotational symmetry the lower branch can be determined. To represent a random assemblage of particles, all models were run using 29 field directions evenly distributed over an octant of the unit sphere. Final simulation results are the average of these directions.

Transient hysteresis loop models were initiated from the zero field step of the major hysteresis loop. The fields were swept back to 200 mT in step of 1 mT. Back-field demagnetization curves were determined from the first-order reversal curve (FORC) simulations of (Nagy et al., 2024), which were similarly simulated at 1 mT resolution. The zero-field steps of reversal curves initiated at negative fields were taken as the remanence steps of the back-field demagnetization curves (*e.g.,* Heslop, 2005).

Collectively, our hysteresis, transient and back-field models constitute ∼4.8 million micromagnetic solutions representing determinations of domain states under varying applied field conditions. Classifying these domain states is not presently feasible and we therefore restrict domain our classification to the 6032 M_{rs} states from the hysteresis loops (16 particle sizes, 13 geometries, and 29 field directions from a Fibonacci distribution). Each of these micromagnetic solutions was classified by visual inspection. Here, we make a distinction between "domain structure", which refers to configuration of the magnetization vectors (*e.g.,* uniformly magnetized, SD, versus SV), and "domain state", which we restrict to refer to an oriented domain structure (*e.g.,* a magnetocrystalline easy axis aligned SV versus a hard aligned SV).

4 Results

4.1 Domain Characterization

From our classification of remanence domain states we identify four main domain structures: SD (uniformly magnetized, including flower structures), SV, s-shaped structures (SS), and multi-vortex (MV). Examples of each of these structures are given in Figure 3.

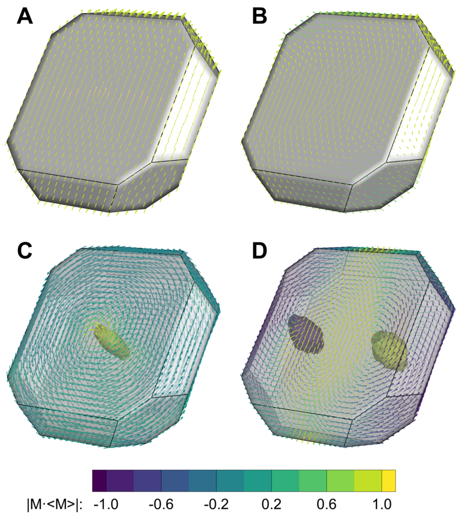

Figure 3. Examples of the main domain structures observed in the remanence states of the hysteresis loop. All particles have an aspect ratio of 0.25. (A) A uniformly magnetized SD structure in a 135 nm particle; (B) An s-shaped structure in a 155 nm particle; (C) An SV structure in a 175 nm particle; (D) An MV structure in a 175 nm particle. The magnetization vectors are colored according to the dot product of the individual vector and the direction of the particles' net magnetization, where the individual vector are normalized unit vectors. In parts C and D, the vortex cores are highlighted by isosurface of relative helicity at 0.95 (yellow) and -0.95 (purple).

The domain structures in our models are predominantly SD and SV, with SS and MV structures only occurring in the largest, most oblate particles. The most frequently occurring domain structures for each of our size/shape combinations are shown in Figure 4A. For small particles ($\lesssim$80 nm), all geometries are SD. At high elongations this extends up to $\sim$120 nm, but for highly oblate particles, the SD region extends up to $\sim$175-185 nm. SV structures prevail above these sizes and SS structures occur for large oblate particles (Figure 4A). We note that our models do not include thermal fluctuations, so it is likely that these SS structures are meta-stable and are likely to rapidly collapse into a more stable structure, which, for these particles, is an SV structure. MV states are only observed in a single model of oblate particles (ESVD = 195 nm, aspect ratio = 0.250) .

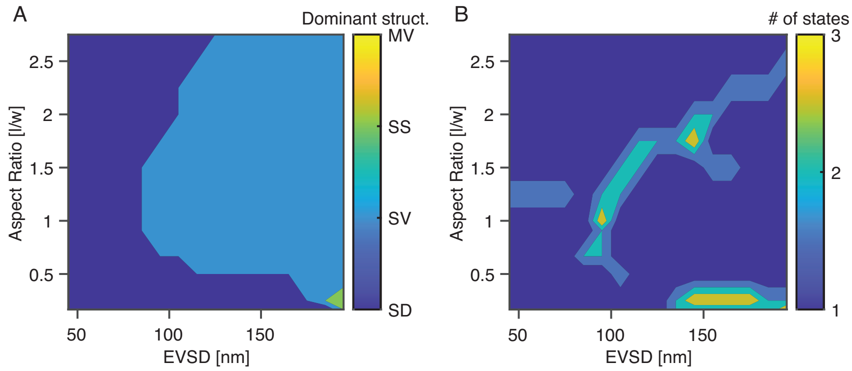

Figure 4. Classification of hysteresis M_{rs} domain structures and states. (A) The most commonly occurring domain structure (SD - single domain, SV - single vortex, SS - s-shaped, MV - multi-vortex). (B) The number of unique domain states.

Within the SD region multiple orientations of magnetization, with respect to the magnetic anisotropy, are observed, which represent different domain states (Figure 4B). For small particles ($\lesssim$80 nm) and moderate elongations, the multiple domain states represents SD structures oriented along either a shape or magnetocrystalline anisotropy easy axis and represents instability in shapes where these anisotropy energies are closely balanced (*i.e.*, aspect ratios ∼1.2–1.3).

For equant particles (aspect ratio of 1), as the particle size increases to 85-105 nm there is a narrow band of particle size that exhibit multiple domains states at remanence (only our 95 nm model has multiple domain states; Figure 4B). This narrow size range corresponds to the short relaxation time and low unblocking temperature unstable zone identified by Nagy et al. (2017).

Across all the different particle geometries the competition between magnetocrystalline or shape anisotropy controlled hard and easy aligned structures is responsible for this domain state multiplicity (Figure 4B). In equant particles, this unstable zone coincides with the transition between SD and SV structures, and is a result of the presence of hard and easy aligned SV structures. For large prolate particles (upper right quadrant of Figure 4B), a large region of domain state multiplicity is observed, with some particles capable of supporting 2-3 different domain states. This is similarly the result of both shape hard- and easy-aligned SV structures. For large oblate particles domain state multiplicity arises from the presence of shape-hard-aligned SV states and shape/magnetocrystalline easy aligned SD states.

4.2 Hysteresis Properties

Our simulations exhibit a wide range of behavior characteristic of SD and SV particles (Figure 5), and bears similarity to the range of behavior seen in hysteresis measurements on natural materials (*e.g.,* Roberts et al., 1995b; Wang & Van der Voo, 2004; Paterson et al., 2018; Nikolaisen et al., 2022).

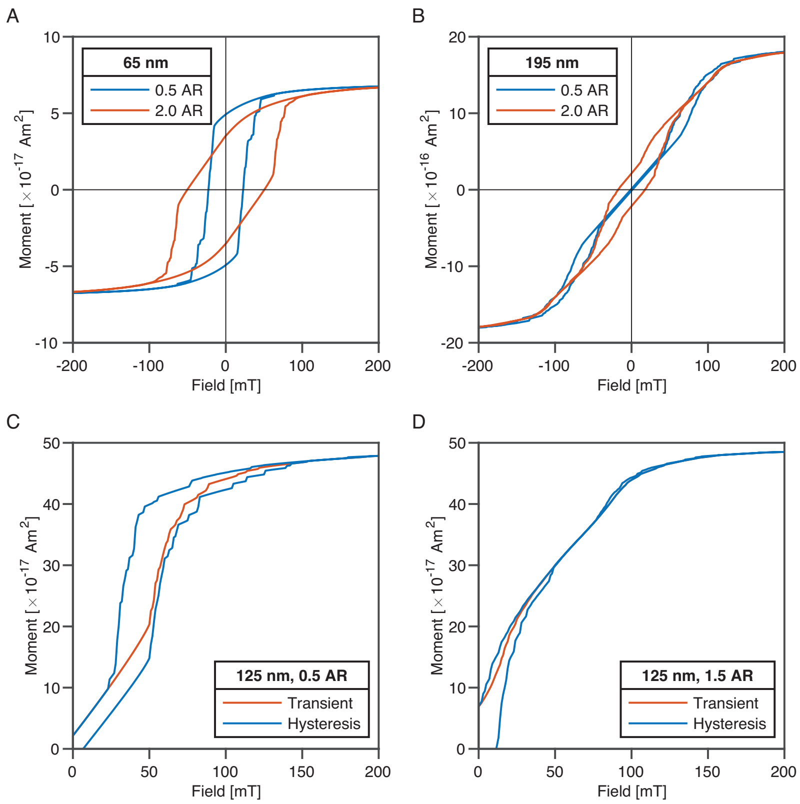

Figure 5. Representative examples of the modeled hysteresis loops for individual particles. (A) Loops from small SD particles. (B) Loops from large SV dominated particles. Transient loop behavior from SV dominated (C) oblate and (D) prolate particles. For the hysteresis loops, only the upper branch was simulated, but was reflected to create a full hysteresis loop.

From our simulations we observe a wide rage of hysteresis shapes from "wasp-waisted" (Figure 6B) to "pot-bellied" (Figure 6C). There is a strong signal from large oblate particles that have extremely wasp-waisted loops and large prolate particles with pot-bellied loops (Figure 6A, B). In general, however, most particles have negative σ_{hys} indicative of pot-bellied behavior, with the most pot-bellied loops coming from prolate particles (AR $\approx$ 1.25–2.00) larger than $\approx$ 130 nm (Figure 6A). Wasp-waistedness is predominantly found in small ($\lesssim$ 80–90 nm) prolate (AR $\sim$ 1.25) particles and larger ($\gtrsim$ 120 nm) oblate particles (AR

$\lesssim$ 0.5). Despite the range of σ_{hys} observed, the median σ_{hys} of the 208 averaged hysteresis loops is $\approx$ -0.56 (interquartile range of -0.74 to -0.14). This is broadly consistent with the experimental observations of Fabian (2003) using sized powders of synthetic titanomagnetite ($\sigma_{\text{hys}} \approx$ -0.9 to -0.5).

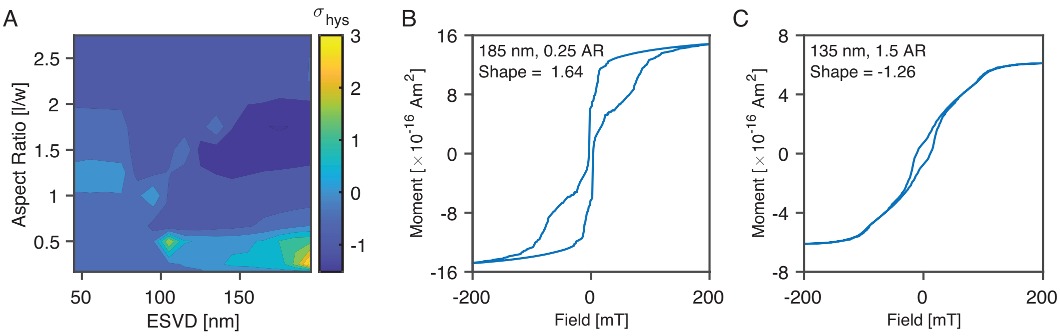

Figure 6. Hysteresis loop σ_{hys} behavior. (A) Contour map of hysteresis σ_{hys} as function of particle size and aspect ratio. Examples of (B) "wasp-waisted" and (C) "pot-bellied" hysteresis loops.

In Figure 7 we show contour plots of hysteresis parameters as a function of particle size and aspect ratio. Transects of these parameters at selected aspect ratios are shown in Figure 8. Small ($\lesssim$ 100 nm) oblate, equant, and prolate particles have M_{rs}/M_s values of 0.707, 0.866, and 0.5, respectively (Figure 7A), which are near the expected values for random assemblages of uniformly magnetized particles dominated by biaxial, cubic, and uniaxial magnetocrystalline anisotropy, respectively, (Dunlop & Özdemir, 1997; Williams et al., 2023). As the particle size increases, prolate particles exhibit a relatively gradual decrease in M_{rs}/M_s to $\sim$0.1 at 195 nm, with equant particles experiencing a slightly steeper decrease (Figure 8A). Oblate particles show the largest decrease of M_{rs}/M_s with increasing particle size (Figures 7A; 8A).

The coercivity (B_c) of the models shows that, for both in the SD and SV states, coercivity increases for increasing prolate particles, as is predicted from SD theory (Stoner & Wohlfarth, 1948) (Figure 7B). For equant particle of $\sim$85–95 nm size, there is a dip in the coercivity to values of $\sim$5 mT, coincident with particles that have low relaxation times (Nagy et al., 2017). This dip in B_c is also seen at all prolate elongations, but occurs at larger particle sizes with increasing elongation. For slightly oblate particles, this low coercivity zone exists in $\sim$85–95 nm particles. Highly oblate particles, however, have consistently low B_c above $\sim$100 nm, which corresponds to the presence on both SD and SV states in these particles.

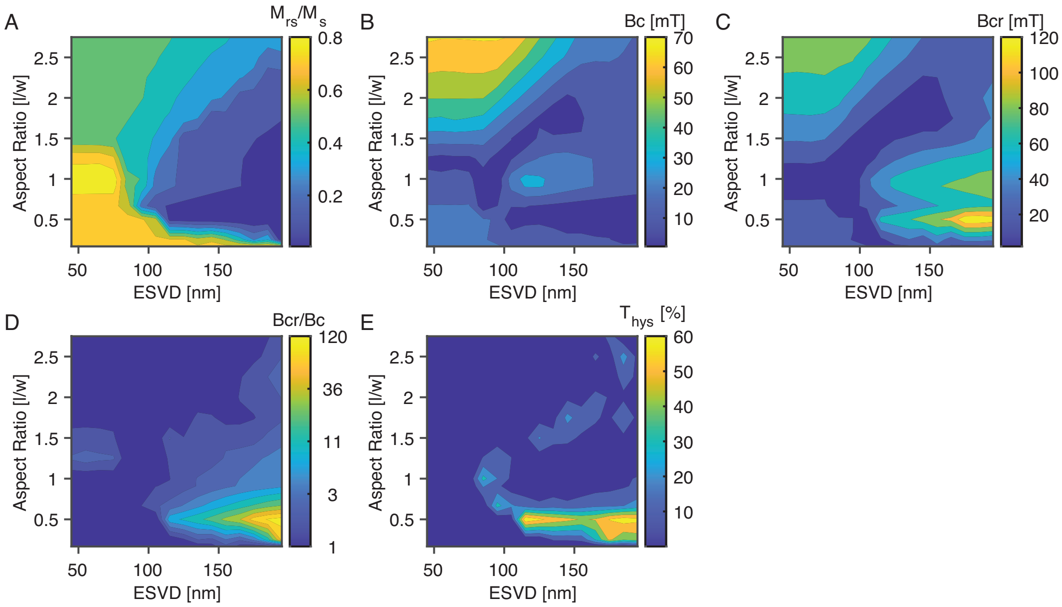

Figure 7. Contour maps of hysteresis properties for random assemblages as function of particle size and aspect ratio. (A) M_{rs}/M_s, (B) B_c, (C) B_{cr}, (D) B_{cr}/B_c, and (E) Transient hysteresis.

Considering B_{cr} (Figure 7C), prolate particles with low B_{cr} values are associated with multiple domain states (Figure 4B); similar to the trend seen for coercivity (Figure 7B). For oblate particles, however, B_{cr} increases with increasing particle size, with the highest values corresponding to particles that are shape-hard-aligned SV in the remanence state. As a result, variations in B_{cr}/B_c are dominated by these states found in oblate particles, which have low B_c and high B_{cr} (Figures 7D). For equant and prolate particles, B_{cr}/B_c remains less than ~ 5, but is consistently below 3 for the smallest particles ($\lesssim 140$ nm; Figure 8D).

Transient hysteresis behavior is related to vortex states nucleating at relatively low fields as the upper branch sweeps to zero-field, but denucleating at higher fields as the transient branch sweeps back to saturation (Yu & Tauxe, 2005). Our SD models consistently have transient loop areas (T_{hys}) that are $<< 1\%$ of the major loop areas (related to numerical noise and a small degree of flowering), while SV states typically have $T_{hys} > 4$–5% (Figure 7E). For a consistent particle geometry, T_{hys} generally increases with increasing particle size (Figure 8E). The most discernible feature of transient hysteresis behavior is the triangular contour region of high T_{hys} (10-70%; Figures 7E and 8E). This occurs from oblate particles across a wide range of sizes (∼100–195nm), but the size range varies with particle geometry for prolate particles. Such large T_{hys} behavior is the result of highly variable SV nucleation and denucleation fields and is an indication that the magnetization and domain state (see Discussion) are strongly dependent on the particles' field pre-history.

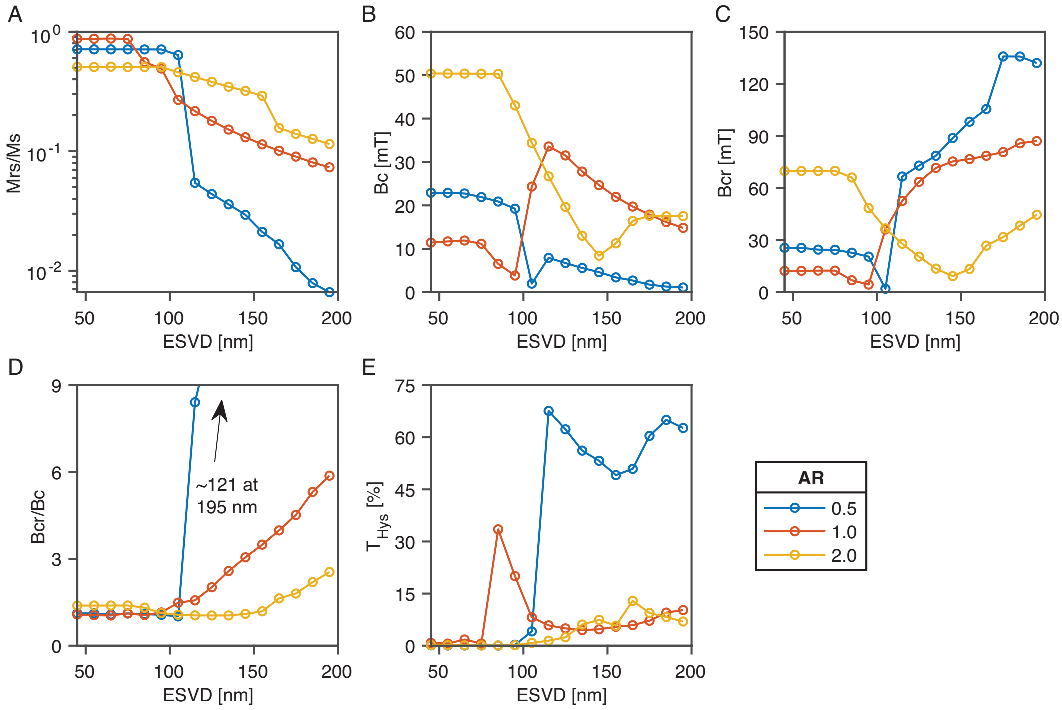

Figure 8. Selected transects through the contours maps shown in Figure 7. (A) M_{rs}/M_s, (B) B_c, (C) B_{cr}, (D) B_{cr}/B_c, and (E) transient hysteresis. The selected aspect ratios are shown in the legend.

5 Discussion

5.1 Comparison with sized data

The effectiveness of the micromagnetic approach at predicting the observed domain structures from single particle microscopy observations has been well demonstrated (*e.g.*, Almeida et al., 2015, 2016; Khakhalova et al., 2018). Only recently, however, have micromagnetic studies been able to systematically model random assemblages of mono-dispersions of large (>100 nm) particles (Nikolaisen et al., 2020, 2022).

In Figure 9 we compare our model derived M_{rs}/M_s, B_c, and B_{cr} values with published hysteresis properties from synthetic samples characterized as magnetite with nominal or known particle sizes. The aim is not to match exact values, but rather compare the range of our simulated results to that of experimental observations. The largest particle we model is 200 nm so the comparison is restricted to experimental data with a reported size <500 nm.

In general, the range of M_{rs}/M_s, B_c, and B_c values from our simulations compares well to those seen in the experimental measurements of sized magnetite particles, which most likely contain distributions of both size and shape (Figure 9). The largest discrepancy is for the oblate particles with aspect ratios of ∼0.5–0.67, where the numerical models predict lower M_{rs}/M_s and B_c values (Figures 7A, B and 9A, B). B_c values show less discrepancy for the oblate particles, but some equant and prolate models have lower B_c values that are not well represented in the experimental data set.

Taking the area mapped out by our simulated results, we can determine the proportion of experimental data that are consistent with our observations (*i.e.,* the 45–195 nm nominally sized specimens that could be explained by a linear combination of one or more of our simulations). For M_{rs}/M_s data, ∼78% fall with the area bounded by our simulations; for B_c and B_{cr}, this is ∼85% ∼67%, respectively. This is a good indication that our model predictions are consistent with experimental observations.

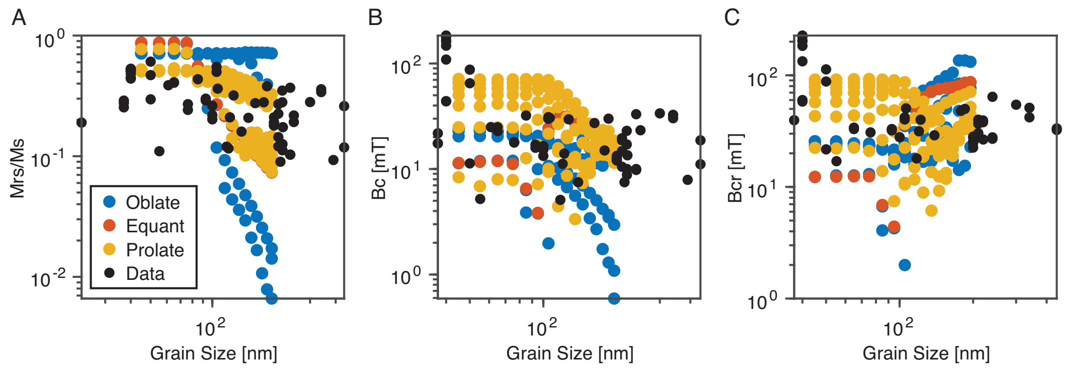

Figure 9. Comparison of model derived hysteresis properties with experimental results from synthetic powders characterized as magnetite with nominal particle sizes. (A) M_{rs}/M_s, (B) B_c, and (C) B_{cr}. Experimental data are for synthetic samples with reported sizes of <500 nm and are taken from Almeida et al. (2015); Argyle & Dunlop (1990); Dunlop (1983, 1986); Krása et al. (2003, 2009, 2011); Levi & Merrill (1978); Muxworthy (1999); Özdemir & Banerjee (1982); Özdemir & O'Reilly (1982); Özdemir et al. (2002); Schmidbauer & Keller (1996); Schmidbauer & Schembera (1987); Smirnov (2009); Yu et al. (2002).

5.2 Distinguishing Magnetic Characteristics

A comprehensive discussion of domain state analysis plots (*i.e.,* the Day plot; Day et al., 1977) using these data, additional micromagnetic simulations, and a more extensive experimental data set are presented in Williams et al. (2023). Here, we restrict the discussion to salient features in whole loop hysteresis data and parameters, discussing the implications for first-order characterization.

In terms of distinguishing dominant domain structure (*i.e.,* SD or SV), M_{rs}/M_s appears to be the most effective parameter: The $M_{rs}/M_s = 0.5$ contour closely follows the SD/SV boundary (*cf.*, Figures 4a and 7A). Out of all sizes and aspect ratios that exhibit only SD and/or SV remanence states (195 our of 208 simulations), only two are predominantly SV with $M_{rs}/M_s \geq 0.5$; the 85 nm particles with aspect ratios of 0.9091 and 1. These particles exhibit only magnetocrystalline hard-axis-aligned vortex states (*e.g.,* Figure 10A), but the vortex core is poorly defined and could also be classified as a twisting flower state (Hertel & Kronmüller, 2002). As a consequence a larger proportion of magnetization is aligned with the vortex core for these 85 nm particles than expected (cf. a well define SV state Figure 10B). These (near) equant particles fall directly in the unstable zone identified by Nagy et al. (2017) and will have extremely short relaxation times; consequently, due to thermal fluctuations $M_{rs}/M_s \approx 0$ (*i.e.,* the particles are “superparamagnetic”).

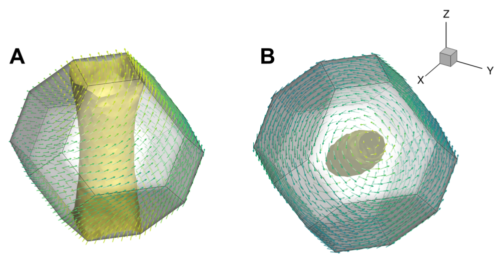

Figure 10. Comparison of SV domain states in equant particles. (A) A hard-aligned vortex in a 85 nm particle and (B) an easy-aligned vortex in a 105 nm particle. Colors are the same as in Figure 3.

The diversity of hysteresis loop shapes is typically attributed to mixing of different particles with contrasting coercivities that arises from mixed mineralogy (*e.g.,* magnetite and hematite) or mixed particle size (*e.g.,* SP and SD) (Roberts et al., 1995a; Tauxe et al., 1996; Fabian, 2003; Frank & Nowaczyk, 2008). Our results, however, are from of magnetite mono-dispersions, and do not contain mixed mineralogy or particle sizes. The diversity of shapes is a result of vortex nucleation/annihilation and/or vortex switching at a range of non-coercivity related fields that are dependent on the field orientation. Although the most extreme shapes are only observed over narrow particle size and geometry ranges, this serves as an important caveat when interpreting hysteresis shape in terms of mixed mineralogy. Similarly, the wide ranging values we observe for SD to SV states means that a similar caution should be considered when interpreting shape in terms of mixing with SP components.

6 Conclusions

In this study we have undertaken the most comprehensive micromagnetic investigation of magnetic hysteresis in magnetite as a function of particle size and shape to date. The range of behavior we observe is consistent with available experimental observations, giving confidence in the robustness of the simulations.

Our models reveal that hysteresis loops from random mono-dispersions can exhibit varied shapes that result from the variability of vortex nucleation and switching depending on the orientation of the field with respect to particle geometry. This is a demonstration that mixed mineralogy or mixed particle sizes are not required to create a diversity of loop shapes.

The size and shape range we model predominantly have SD and SV remanence domain structures. An M_{rs}/M_s value of 0.5 is the boundary between these structures. The SV structures observed, exhibit both easy- and hard-aligned domain states, with the hard aligned states corresponding to the unstable magnetic carriers identified by Nagy et al. (2017).

We have identified distinct size and shape combinations that yield low B_c and B_{cr}, indicating low stability particles. These combinations, particularly for B_c, have a correspondence to particles with a higher number of possible domain states, but this relation is less clear for highly prolate particles larger than ∼150 nm.

The area of the transient hysteresis loop, which is rarely measured, has a strong relation to particles that have multiple possible domain states. For transient hysteresis, however, the contrast is more distinct than for B_c and B_{cr}, suggesting that it potentially offers a greater discrimination of behavior likely responsible for unstable paleomagnetic recorders.

7 Open Research

All results reported here were generated using the open source micromagnetic modeling code of Ó Conbhuí et al. (2018) and Williams et al. (n.d.). Source code for MERRILL is available at `https://bitbucket.org/wynwilliams/merrill/` and is provided under a CC-BY-SA 4.0 International license. Additional MERRILL resources are available at `https://rockmag.org`. All model data presented here and example MERRILL input scripts and Treilis geometry generation scripts to reproduce these models are available at Paterson et al. (2024).

Acknowledgments

G.A.P. acknowledges funding from Natural Environmental Research Council (NERC) Independent Research Fellowship (NE/P017266/1) and grant NE/W006707/1; W.W. and

A.R.M. acknowledges support from NERC grants NE/S001018/1 and NE/V001388/1. L.T., W.W. and L.N. acknowledge support of NSFGEO-NERC grant EAR1827263. L.N. acknowledges funding from Natural Environmental Research Council (NERC) Independent Research Fellowship (NE/V014722/1).

References

Almeida, T. P., Muxworthy, A. R., Kasama, T., Williams, W., Damsgaard, C., Frandsen, C., . . . Dunin-Borkowski, R. E. (2015). Effect of maghemization on the magnetic properties of nonstoichiometric pseudo-single-domain magnetite particles. *Geochem. Geophys. Geosyst.*, *16*, 2969-2979. doi: 10.1002/2015GC005858

Almeida, T. P., Muxworthy, A. R., Kovács, A., Williams, W., Nagy, L., Conbhuí, P. Ó., . . . Dunin-Borkowski, R. E. (2016). Direct observation of the thermal demagnetization of magnetic vortex structures in nonideal magnetite recorders. *Geophys. Res. Lett.*, *43*, 8426-8434. doi: 10.1002/2016gl070074

Argyle, K. S., & Dunlop, D. J. (1990). Low-temperature and high-temperature hysteresis of small multidomain magnetites (215–540 nm). *J. Geophys. Res.*, *95*, 7069-7082. doi: 10.1029/JB095iB05p07069

Coreform LLC. (2017). *Coreform Cubit, v16.4 (64-Bit).* Retrieved from `https://coreform.com`

Day, R., Fuller, M. D., & Schmidt, V. A. (1977). Hysteresis properties of titanomagnetites: Grain-size and compositional dependence. *Phys. Earth Planet. Inter.*, *13*, 260-267. doi: 10.1016/0031-9201(77)90108-X

Dunlop, D. J. (1983). Viscous magnetization of 0.04 - 100 μm magnetites. *Geophys. J. R. Astr. Soc.*, *74*, 667-687. doi: 10.1111/j.1365-246X.1983.tb01899.x

Dunlop, D. J. (1986). Hysteresis properties of magnetite and their dependence on particle size: A test of pseudo-single-domain remanence models. *J. Geophys. Res.*, *91*, 9569-9584. doi: 10.1029/JB091iB09p09569

Dunlop, D. J. (2002). Theory and application of the Day plot (Mrs/Ms versus Hcr/Hc) 1. Theoretical curves and tests using titanomagnetite data. *J. Geophys. Res.*, *107*, 2056. doi: 10.1029/2001JB000486

Dunlop, D. J., & Özdemir, Ö. (1997). *Rock magnetism: Fundamentals and frontiers* (Vol. 3). New York: Cambridge University Press.

Fabian, K. (2003). Some additional parameters to estimate domain state from isothermal magnetization measurements. *Earth Planet. Sci. Lett.*, *213*, 337-345. doi: 10.1016/S0012-821X(03)00329-7

Fabian, K., & von Dobeneck, T. (1997). Isothermal magnetization of samples with stable preisach function: A survey of hysteresis, remanence, and rock magnetic parameters. *J. Geophys. Res.*, *102*, 17659-17677. doi: 10.1029/97JB01051

Frank, U., & Nowaczyk, N. R. (2008, 11). Mineral magnetic properties of artificial samples systematically mixed from haematite and magnetite. *Geophysical Journal International*, *175*(2), 449-461. doi: 10.1111/j.1365-246X.2008.03821.x

Hertel, R., & Kronmüller, H. (2002). Finite element calculations on the single-domain limit of a ferromagnetic cube - a solution to μmag standard problem no. 3. *Journal of Magnetism and Magnetic Materials*, *238*(2), 185-199. doi: 10.1016/S0304-8853(01)00876-9

Heslop, D. (2005). A Monte Carlo investigation of the representation of thermally activated single-domain particles within the day plot. *Studia Geophysica Et Geodaetica*, *49*(2), 163-176.

Jackson, M., & Solheid, P. (2010). On the quantitative analysis and evaluation of magnetic hysteresis data. *Geochem. Geophys. Geosyst.*, *11*, Q04Z15. doi: 10.1029/2009GC002932

Khakhalova, E., Moskowitz, B. M., Williams, W., Biedermann, A. R., & Solheid, P. (2018). Magnetic vortex states in small octahedral particles of intermediate titanomagnetite. *Geochem. Geophys. Geosyst.*, *19*, 3071-3083. doi: 10.1029/2018gc007723

Krása, D., Heunemann, C., Leonhardt, R., & Petersen, N. (2003). Experimental procedure to detect multidomain remanence during thellier-thellier experiments. *Phys. Chem. Earth*, *28*, 681-687. doi: 10.1016/S1474-7065(03)00122-0

Krása, D., Muxworthy, A. R., & Williams, W. (2011). Room- and low-temperature magnetic properties of 2-d magnetite particle arrays. *Geophys. J. Int.*, *185*, 167-180. doi: 10.1111/j.1365-246X.2011.04956.x

Krása, D., Wilkinson, C. D. W., Gadegaard, N., Kong, X., Zhou, H., Roberts, A. P., ... Williams, W. (2009). Nanofabrication of two-dimensional arrays of magnetite particles for fundamental rock magnetic studies. *J. Geophys. Res.*, *114*, B02104. doi: 10.1029/2008JB006017

Lascu, I., Einsle, J. F., Ball, M. R., & Harrison, R. J. (2018). The vortex state in geologic materials: A micromagnetic perspective. *J. Geophys. Res.*, *123*(9), 7285-7304. doi: 10.1029/2018JB015909

Levi, S., & Merrill, R. T. (1978). Properties of single-domain, pseudo-single-domain, and multidomain magnetite. *J. Geophys. Res.*, *83*, 309-323. doi: 10.1029/JB083iB01p00309

Muxworthy, A. R. (1999). Low-temperature susceptibility and hysteresis of magnetite. *Earth Planet. Sci. Lett.*, *169*, 51-58. doi: 10.1016/S0012-821X(99)00067-9

Nagy, L., Moreno, R., Muxworthy, A. R., Williams, W., Paterson, G. A., Tauxe, L., & Valdez-Grijalva, M. A. (2024). Micromagnetic determination of the forc response of paleomagnetically significant magnetite assemblages. *ESS Open Archive*. doi: ???

Nagy, L., Williams, W., Muxworthy, A. R., Fabian, K., Almeida, T. P., Ó Conbhuí, P., & Shcherbakov, V. P. (2017). Stability of equidimensional pseudo–single-domain magnetite over billion-year timescales. *Proc. Nat. Acad. Sci. U.S.A.*, *114*, 10356-10360. doi: 10.1073/pnas.1708344114

Nikolaisen, E. S., Harrison, R., Fabian, K., Church, N., McEnroe, S. A., Sørensen, B. E., & Tegner, C. (2022). Hysteresis parameters and magnetic anisotropy of silicate-hosted magnetite exsolutions. *Geophys. J. Int.*, *229*, 1695-1717. doi: 10.1093/gji/ggac007

Nikolaisen, E. S., Harrison, R. J., Fabian, K., & McEnroe, S. A. (2020). Hysteresis of natural magnetite ensembles: Micromagnetics of silicate-hosted magnetite inclusions based on focused-ion-beam nanotomography. *Geochem. Geophys. Geosyst.*, *21*, e2020GC009389. doi: 10.1029/2020GC009389

Ó Conbhuí, P., Williams, W., Fabian, K., Ridley, P., Nagy, L., & Muxworthy, A. R. (2018). Merrill: Micromagnetic earth related robust interpreted language laboratory. *Geochem. Geophys. Geosyst.*, *19*, 1080-1106. doi: 10.1002/2017gc007279

Özdemir, Ö., & Banerjee, S. K. (1982). A preliminary magnetic study of soil samples from west-central minnesota. *Earth Planet. Sci. Lett.*, *59*, 393-403. doi: 10.1016/0012-821X(82)90141-8

Özdemir, Ö., Dunlop, D. J., & Moskowitz, B. M. (2002). Changes in remanence, coercivity and domain state at low temperature in magnetite. *Earth Planet. Sci. Lett.*, *194*, 343-358. doi: 10.1016/S0012-821X(01)00562-3

Özdemir, Ö., & O'Reilly, W. (1982). An experimental study of the intensity and stability of thermoremanent magnetization acquired by synthetic monodomain titanomagnetite substituted by aluminium. *Geophys. J. R. Astr. Soc.*, *70*, 141-154. doi: 10.1111/j.1365-246X.1982.tb06396.x

Paterson, G. A., Moreno Ortega, R., Muxworthy, A. R., Nagy, L., Williams, ., W., & Tauxe, L. (2024). Micromagnetic hysteresis results for magnetite [dataset]. *Zenodo*. doi: 10.5281/zenodo.10355842

Paterson, G. A., Muxworthy, A. R., Yamamoto, Y., & Pan, Y. (2017). Bulk magnetic domain stability controls paleointensity fidelity. *Proceedings of the National Academy of Sciences*, *114*, 13120-13125. doi: 10.1073/pnas.1714047114

Paterson, G. A., Zhao, X., Jackson, M., & Heslop, D. (2018). Measuring, processing, and analyzing hysteresis data. *Geochem. Geophys. Geosyst.*, *19*, 1925-1945. doi: 10.1029/2018GC007620

Rave, W., Fabian, K., & Hubert, A. (1998). Magnetic states of small cubic particles with uniaxial anisotropy. *Journal of Magnetism and Magnetic Materials*, *190*(3), 332-348. doi:

10.1016/S0304-8853(98)00328-X

Rivas, J., Zamarro, J., Martin, E., & Pereira, C. (1981). Simple approximation for magnetization curves and hysteresis loops. *IEEE Trans. Magn.*, *17*, 1498-1502. doi: 10.1109/TMAG.1981.1061241

Roberts, A. P., Cui, Y., & Verosub, K. L. (1995a). Wasp-waisted hysteresis loops: Mineral magnetic characteristics and discrimination of components in mixed magnetic systems. *J. Geophys. Res.*, *100*, 17909-17924. doi: 10.1029/95JB00672

Roberts, A. P., Cui, Y., & Verosub, K. L. (1995b). Wasp-waisted hysteresis loops: Mineral magnetic characteristics and discrimination of components in mixed magnetic systems. *J. Geophys. Res.*, *100*(B9), 17909-17924. doi: 10.1029/95JB00672

Roberts, A. P., Tauxe, L., Heslop, D., Zhao, X., & Jiang, Z. (2018). A critical appraisal of the "Day" diagram. *J. Geophys. Res.*, *123*, 2618-2644. doi: 10.1002/2017JB015247

Schabes, M. E., & Bertram, H. N. (1988). Magnetization processes in ferromagnetic cubes. *Journal Of Applied Physics*, *64*(3), 1347 – 1357.

Schmidbauer, E., & Keller, R. (1996). Magnetic properties and rotational hysteresis of Fe_3O_4 and γ-Fe_2O_3 particles $\sim$ 250 nm in diameter. *J. Magn. Magn. Mater.*, *152*, 99-108. doi: 10.1016/0304-8853(95)00446-7

Schmidbauer, E., & Schembera, N. (1987). Magnetic hysteresis properties and anhysteretic remanent magnetization of spherical Fe_3O_4 particles in the grain size range 60–160 nm. *Phys. Earth Planet. Inter.*, *46*, 77-83. doi: 10.1016/0031-9201(87)90173-7

Smirnov, A. V. (2009). Grain size dependence of low-temperature remanent magnetization in natural and synthetic magnetite: Experimental study. *Earth Planets Space*, *61*, 119-124. doi: 10.1186/bf03352891

Stoner, E. C., & Wohlfarth, E. P. (1948). A mechanism of magnetic hysteresis in heterogeneous alloys. *Philosophical Transactions of the Royal Society of London. Series A, Mathematical and Physical Sciences*, *240*, 599–642. doi: 10.1098/rsta.1948.0007

Tauxe, L., Mullender, T. A. T., & Pick, T. (1996). Potbellies, wasp-waists, and superparamagnetism in magnetic hysteresis. *J. Geophys. Res.*, *101*, 571-583. doi: 10.1029/95JB03041

von Dobeneck, T. (1996). A systematic analysis of natural magnetic mineral assemblages based on modelling hysteresis loops with coercivity-related hyperbolic basis functions. *Geophys. J. Int.*, *124*, 675-694. doi: 10.1111/j.1365-246X.1996.tb05632.x

Wang, D., & Van der Voo, R. (2004). The hysteresis properties of multidomain magnetite and titanomagnetite/titanomaghemite in mid-ocean ridge basalts. *Earth Planet. Sci. Lett.*, *220*(1), 175-184. doi: 10.1016/S0012-821X(04)00052-4

Williams, W., & Dunlop, D. J. (1989). Three-dimensional micromagnetic modelling of ferromagnetic domain structure. *Nature*, *337*, 634-637. doi: 10.1038/337634a0

Williams, W., & Dunlop, D. J. (1995). Simulation of magnetic hysteresis in pseudo-single-domain grains of magnetite. *J. Geophys. Res.*, *100*(B3), 3859-3871. doi: 10.1029/94JB02878

Williams, W., Fabian, K., P., R., Nagy, L., Paterson, G., & Muxworthy, A. R. (n.d.). *Merrill* [webpage]. Retrieved from `https://bitbucket.org/wynwilliams/merrill`

Williams, W., Moreno, R., Muxworthy, A. R., Paterson, G. A., Nagy, L., Tauxe, L., … Ferreira, I. (2023). Vortex magnetic domain state behavior in the day plot. *ESS Open Archive*. doi: 10.22541/essoar.170365251.19347068/v1

Williams, W., Muxworthy, A. R., & Paterson, G. A. (2006). Configurational anisotropy in single-domain and pseudosingle-domain grains of magnetite. *J. Geophys. Res.*, *111*(B12). doi: 10.1029/2006JB004556

Yu, Y., Dunlop, D. J., & Özdemir, Ö. (2002). Partial anhysteretic remanent magnetization in magnetite 1. additivity. *J. Geophys. Res.*, *107*, EPM 7-1-EPM 7-9. doi: 10.1029/2001JB001249

Yu, Y., & Tauxe, L. (2005). On the use of magnetic transient hysteresis in paleomagnetism for granulometry. *Geochem. Geophys. Geosyst.*, *6*. doi: 10.1029/2004GC000839

Yu, Y., & Tauxe, L. (2008). Micromagnetic models of the effect of particle shape on magnetic hysteresis. *Physics of the Earth and Planetary Interiors*, *169*(1), 92-99. doi: 10.1016/j.pepi.2008.07.006

Zhao, X., Roberts, A. P., Heslop, D., Paterson, G. A., Li, Y., & Li, J. (2017). Magnetic domain state diagnosis using hysteresis reversal curves. *J. Geophys. Res.*, *122*. doi: 10.1002/2016JB013683